

The Reduction Mechanisms of Zinc Oxide Solid Solutions

Lee Fui Tong

School of Engineering, Monash University Malaysia,
No. 2, Jalan Kolej, Bandar Sunway, 46150 Petaling Jaya,
Selangor Darul Ehsan, Malaysia.

Abstract : The reduction of dense zinc oxide (ZnO) solid solutions in CO/CO₂ and CO/N₂ gas mixtures has been investigated at temperatures between 900 and 1100 °C. The microstructural characterization of the reacted and partially reduced samples was complemented with measurements of the rates of the reactions. The kinetics of reduction of zinc oxide was found to be dependent upon the CO partial pressure, temperature, degree of reduction, and the type of impurity oxides (i.e. FeO, MgO, CaO, SiO₂, MnO, Al₂O₃) present in the samples. The reduction of ZnO solid solutions resulted in the formation of elongated pore tunnels at the reaction interface and a porous product layer composed of impurity oxide added. An interface reaction model has been proposed for the observed reaction kinetics and product microstructures formed for the reduction of ZnO solid solutions. From the analysis of the relative rates of the various chemical reactions and mass transport processes, the rates of reduction of ZnO with and without impurity oxide addition were found to be controlled jointly by chemical reaction at the ZnO reaction interface and pore diffusion of reducing gas through the porous reaction product layer.

Keywords : ZnO Solid Solutions, Pure ZnO, Microstructures, Reaction rates, Reduction Mechanisms,

Abstrak : Proses penurunan untuk larutan pepejal zink oksida tumpat (ZnO) dalam campuran gas CO/CO₂ dan CO/N₂ telah dikaji pada suhu diantara 900 dan 1100 °C. Sifat mikrostruktur dari sampel separa terturun yang sudah bertindak telah dilengkapi dengan ukuran-ukuran kadar tindak balas. Kinetik penurunan didalam zink oksida telah didapati bergantung kepada tekanan separa CO, suhu, kadar penurunan, dan jenis oksida bendasing (iaitu FeO, MgO, CaO, SiO₂, MnO, Al₂O₃) yang ada didalam sampel. Proses penurunan untuk larutan pepejal zink oksida (ZnO) menghasilkan pembentukan perpanjangan liang terowong di antara muka tindak balas dan satu lapisan keluaran berliang mengandungi tambahan oksida bendasing. Satu model tindak balas antara muka telah dicadangkan untuk memerhati kinetik tindak balas dan pengeluaran mikrostruktur untuk penurunan larutan pepejal ZnO. Analisa kadar nisba keatas berbagai-bagai tindak balas kimia dan proses pengangkutan jisim, kadar penurunan zink oksida yang ada dan tidak ada tambahan oksida bendasing telah didapati dikawal bersama oleh tindak balas kimia di antara muka tindak balas zink oksida dan resapan liang dari gas penurun melalui lapisan zink oksida berliang atau lapisan tindak balas pengeluaran.

Received 19.06.01; accepted 2.01.02

Introduction

Despite the industrial importance of the ZnO–CO or ZnO–C systems, there have been relatively few studies on the mechanisms and kinetics of reduction of zinc oxide solid solutions with carbon and carbon monoxide gas. Many aspects of the reaction product morphologies and reaction kinetics during the reduction process at various gas mixtures and temperatures are poorly understood. Therefore, detailed study of the reduction mechanism of ZnO will add valuable information to the reduction behavior of the primary zincite phases in zinc blast furnace sinter microstructure.

There are no known published works done on the reduction of zinc oxide with controlled amount of impurity oxide that is homogeneously dissolved in its solid solution. Jones and Davis [1] investigated the reduction of ZnO and strontium oxide powder mixtures in various proportion (for e.g., the ratio of SrO:ZnO = 2.5:1) by CO in the temperature range from 500 to 850 °C. The SrO added was not chemically incorporated into the

solid solution in the ZnO phase but formed a fine mixture of separate ZnO and SrO phases. The reduction rates of ZnO were found to be an order of magnitude greater in the presence of SrO. It was concluded that the reduction rate of ZnO by CO is controlled by gaseous diffusion processes and it was suggested that the enhanced rate of reduction of ZnO with SrO addition resulted from the complete removal of one of the reaction products, CO₂, to form SrCO₃.

Guger and Manning [2] studied the reduction kinetics of ZnO with CO gas in the temperature range of 1000 °C to 1500 °C at atmospheric pressure. They showed that the reduction of reasonable dense, pure ZnO pellets with CO can be adequately described by a mixed regime model, which postulates an external diffusion step acting in series with a first order irreversible chemical reaction step at the surface.

Lee & Hayes [3] studied the reduction of dense pure ZnO samples in CO/CO₂/N₂ gas mixtures between 900 °C and 1100 °C and showed that mechanisms and kinetics of reduction were found to be dependent upon CO partial pressure, oxygen potential of the gas mixtures, temperature and degree of reduction. It was also concluded that the rate of reduction of pure ZnO was controlled jointly by chemical reaction at the ZnO surface and pore diffusion of reducing gas through the porous ZnO layer. This interpretation differs with the mixed-regime model postulated by Guger & Manning [2].

This paper examines the mechanisms and kinetics of reduction of ZnO solid solutions containing 1wt% of (MgO, CaO, SiO₂, MnO, FeO, Al₂O₃ respectively) carried out at temperatures in the range of 900 °C to 1100 °C, under a wide range of CO/CO₂, CO/N₂, and CO/CO₂/N₂ gas mixtures.

Experimental

Sample Preparation

All the samples used in the present investigation were prepared from high purity, ultra-fine powdered oxides (ZnO, CaO, SiO₂, MgO, MnO, Al₂O₃) of particle sizes in the range 30 µm to 50 µm. The wustite (FeO) powder used for iron impurity additions studies in ZnO solid solution was prepared by oxidizing high purity iron powder in CO/CO₂=1 and N₂ gas mixtures at 1200 °C for 3 days.

Accurately weighed mixtures of powders were ground in an agate mortar before placing them in a 15 mm diameter steel die, and compressing the powder at 200 MPa into cylindrical pellets. The pellets were sintered in air for 24 hours at the peak temperature of 1250 °C in a muffle furnace. Upon completion of sintering, the furnace was turned off, and the specimen were allowed to furnace cool until the temperature reached 1000 °C, the specimen was then cooled in air to room temperature. This produced cylindrical pellets of about 13 mm in diameter, average thickness of 1.00 mm and a density of approximately 5.43 g cm⁻³ (98% theoretical density). SEM examination verified that the samples contained little or no porosity with no connected pores (Appendix 1). The impurity content of the ZnO solid solutions was independently checked by chemical analysis and electron microprobe analysis on the polished sample surfaces, and in all cases the checks agreed with the relative proportions of the reactants initially added to the mixture for sintering, i.e., the impurity oxide added was not evaporated or vaporized under this heating environment condition.

To obtain the same size of sample for each experiment the pellets were first polished on both sides on 600 mesh sized SiC paper until a thickness of 1.0 mm was obtained. The polished pellets were then evenly covered with polymethyl-methacrylate

(PMMA), and using 2 glass slides the samples were mounted with surfaces parallel to the polished faces of the sample. Blocks containing excess PMMA were ground off and then fixed to glass slide using araldite resin. The samples were cut into 1.0-mm strips using a Diamond Watering Blade and successive sample positions being set with the in-built micrometer. The parallel saw cuts were filled with PMMA to provide support for the sample and the blocks were then cut at right angles to the original cuts again into 1.0 mm strips. The PMMA and araldite were then dissolved in acetone to expose the 1.0 mm x 1.0 mm x 1.0 mm samples for kinetics studies in a reduction furnace. Typical cube-shaped sample weights ranged from 5.50 x 10⁻³ g to 5.80 x 10⁻³ g.

Procedure

The surface and product morphologies formed during the reduction of zinc oxides were studied using a technique involving the reduction of 1 mm cube-shaped samples in a high velocity gas stream followed by rapid quenching in liquid nitrogen [4, 5].

The techniques adopted in the present investigations were devised to fulfill three specific requirements;

- (i) to minimize the difference between the bulk gas composition and that at the sites of the chemical reactions on the oxide specimens,
- (ii) to provide dense, uniform and reproducible samples in order that any microstructural changes could be detected and characterized, and
- (iii) the provision of a facility for rapid quenching of samples from the reaction temperature allows partially reduced samples to be examined without risk of contamination or modification during cooling.

The rate measurements were made at temperatures from 900 to 1100 °C. Each point in the plot between percentage reduction and time (e.g., Figure 1) represents one reduction experiment for a given reaction condition. Partially reduced product microstructures were examined using the Phillips 505 scanning electron microscope (SEM), and the effects of the following conditions on reaction kinetics, i.e., (i) reaction temperature, (ii) time, (iii) degree of reduction, (iv) type of impurity oxide addition, and (v) reducing gas composition were studied.

Results

ZnO Solid Solution Synthesis

The addition of impurity oxides to ZnO resulted in the formation of a single-phase microstructure – i.e., a solid solution. Depending on the type of impurity oxide addition, extra care was taken to ensure sufficient time for diffusion under a controlled high temperature oxidizing environment to put all the oxide additions in solution in ZnO to

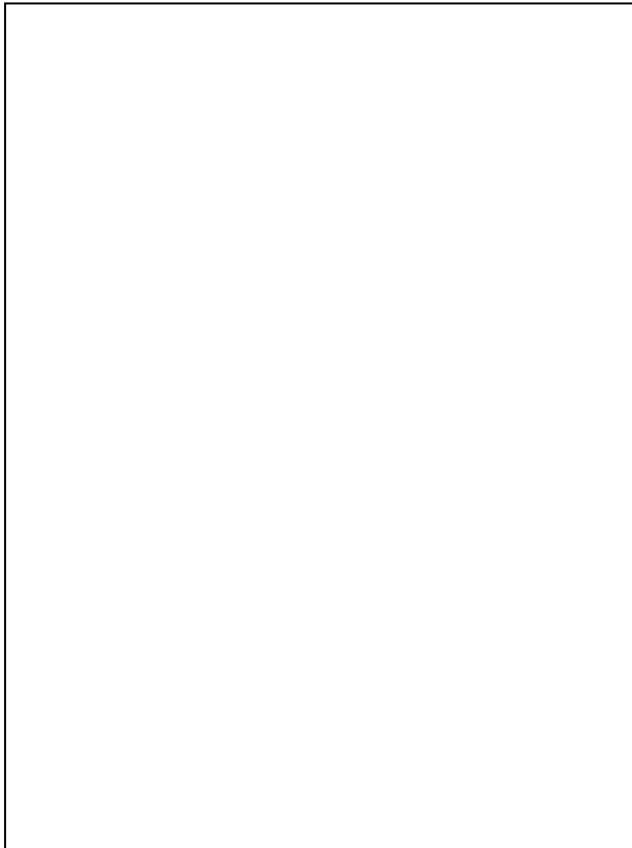


Figure 1. Effect of 1wt% oxide additions on the reduction behavior of ZnO by CO gas at (a) 900°C and (b) 1100°C

produce a single phase homogenize compositional structure. The experimental techniques employed in this study have allowed virtually all the added impurity oxides (1 wt%) to be incorporated into the ZnO lattice structure as evidenced by metallography & SEM observations. Some typical examples of the dense single-phase ZnO solid solution micrographs were shown in Appendix 1. The presence of a single-phase microstructure observed (with no or very little fine pores) clearly showed that a ZnO solid solution was formed with no evidence of a two-phase structure. Under EDX scan on the entire surface of the polished samples shown in Appendix 1 (a-b), no trace of FeO or MnO precipitates was detected. Additionally from SEM micrographs (Appendix 1(c-d)), it is also evidenced that the ZnO solid solution produced is a dense structure consisting of one single phase. For example, the pores observed in ZnO + 1wt% CaO are isolated pores and are not connected. Using Philips 505 SEM-EDX imaging scan on fractured sample surfaces also showed no evidence of isolated concentration of a separate impurity oxide precipitate phase or grain in between the larger ZnO grains, which therefore further indicated that the 1wt% impurity oxide added is homogeneously incorporated into the ZnO solid solution. Further evidence of the production of single-phase dense ZnO solid solution can be readily observed in the unreacted core of the partially reduced ZnO solid solution samples in Figure 3. Earlier studies by the

author (Lee [11]) has also shown that the maximum solubility of FeO in ZnO is about 22wt% at 1575°C whereas at room temperature, FeO can be fully dissolved into the ZnO lattice structure with concentration > 5wt%. Sintering under a high temperature oxidizing environment induced rapid & complete dissolution of the small amount of impurity oxide added into the ZnO lattice structure; and upon fast quenching in air, all of the dissolved & homogenized impurities, is trapped in the lattice structure even if the solubility limit of ZnO solvus line is exceeded at room temperature (Lee [5]). Additionally, XRD work from previous studies (Lee [5]) also confirmed single phase of ZnO with no trace or any peaks of the added metallic oxide phase.

Kinetics Measurements

Figure 1 shows the summarized form of the reduction behavior of ZnO solid solutions containing 1 wt% of MgO, CaO, FeO, SiO₂, Al₂O₃ and MnO. A more detailed analysis of the reduction kinetics and behavior of ZnO solid solutions studied at temperature ranged from 900 to 1100 °C at various CO/CO₂/N₂ gas mixtures was described elsewhere by the author [3, 5]. The addition of 1 wt% of CaO, MnO and SiO₂ dissolved in the ZnO phase enhances the reduction rate relative to pure ZnO, but the relative rate of increase becomes less marked with increasing reduction temperature. On the other hand, the reduction rate of ZnO is decreased by the presence of MgO, Al₂O₃ and FeO dissolved in the ZnO phase over the temperature range from 900 to 1100 °C. These results show that the reductions of zinc oxide are sensitive to the presence of small amounts of dissolved impurities incorporated into the crystal planes in the hexagonal ZnO HCP-crystal structure.

All of the plots generally show that the reduction exhibit an initial linear rate up to 30% reduction followed by a decreased in reduction rate with the progress of reduction. For all the CO/N₂, CO/CO₂ & CO/CO₂/N₂ gas mixtures and impurities studied (Lee [5]), the initial linear rates are maintained to higher % reduction at higher reduction temperatures and lower P_{CO}.

Figure 2 shows the summaries of all the reaction rate data obtained from ZnO containing 1 wt% of FeO, MgO, CaO, SiO₂, MnO and Al₂O₃ respectively plotted against CO partial pressure in CO/CO₂/N₂ gas mixtures at varying reduction temperatures. Inspection of these curves shows that the rate of reduction increases with increasing reduction temperature for a given P_{CO}. Higher initial reduction rates are also observed with N₂ than CO₂ additions, when compared at equivalent CO partial pressures. The relative differences in the initial reduction rates between CO/N₂ and CO/CO₂



Figure 2. Partial pressure effects on the initial reduction rates of ZnO + 1wt% of (a) FeO, (b) MgO, (c) CaO, (d) SiO₂, (e) MnO, and (f) Al₂O₃. Closed symbols (■, ▲, ●) → CO/N₂ gas mixtures and Opened symbols (□, △, ○) → CO/CO₂ gas mixtures.

gas mixtures appear to be greater at lower CO partial pressures ($P_{CO} < 0.2$ atm).

Table 1 summarizes the effects of impurity oxides on the initial reduction rate of ZnO in the temperature range from 900 to 1100 °C. In all the impurity oxides studied, the presence of CaO and MnO in ZnO solid solution appears to show the greatest increases in the reduction rate of ZnO at all temperature range studied. The additions of MgO, FeO, and Al₂O₃ significantly decelerate the reaction rates when the samples were reduced in pure CO or CO/CO₂/N₂ gas mixtures at temperature ≥ 1000 °C, while at a lower temperature (900 °C) the presence of MgO and Al₂O₃ appears to retard reduction compared with pure ZnO reduction rates.

Microstructure

Figure 3 shows typical example of SEM micrographs of partially reduced ZnO solid solutions (i.e. containing 1wt% of FeO, CaO, SiO₂,

MgO and MnO). This type of product morphologies involves the continuous growth of the product phase at the reaction interface, forming connected longitudinal pore structure which provide an easy gas access to the advancing reaction interface. Earlier studied by the author [5] showed that the pore sizes increase with increasing distance from the reaction interface towards the external sample surface. The pores were initially oriented perpendicular to the reaction interface within each crystal grain but this directionality was gradually lost in the coarser pore structure away from the reaction interface. The built up of reaction product layer in thickness with the progress of reduction also contributed to the increase in the gaseous diffusional resistance, which therefore decreases the rate of reduction as evident by the microstructural observations of reduced ZnO solid solutions samples and by the curvature behavior of the %reduction–time plots.



Figure 3. Typical SEM micrographs at reaction interface produced on reduction of ZnO solid solutions. (a) 1wt% FeO, 1000^oC, 1 min., 100% CO; (b) 1wt% MnO, 1000^oC, 1 min., 20%CO-80%N₂; (c) 1wt% SiO₂, 900^oC, 5 min., 25%CO-75%CO₂; (d) 1wt% MgO, 1000^oC, 5 min., 5%CO-95%N₂; (e) 1wt% CaO, 1000^oC, 1min., 75%CO-25%CO₂; (f) 1wt% Al₂O₃, 1000^oC, 5 min., 50%CO-50%N₂.

Temperature	Gas Mixtures	Initial Rate Measurements (wt.% reduction per minute)						
		MgO	CaO	SiO ₂	MnO	Al ₂ O ₃	FeO	Pure
900 °C	100% CO	1.0	17	7	6.4	2.2	6.3	4.2
	CO/CO ₂ =1	1.8	2.0	3.8	2.5	1.6	2.8	2.0
	CO/N ₂ =1	0.7	11.8	4.2	3.8	1.5	4	1.7
1000 °C	100% CO	5.6	43.5	22	28.7	11.6	13.5	16.2
	CO/CO ₂ =1	4.1	11.4	12.2	11.1	8.2	3.5	9.1
	CO/N ₂ =1	4.3	32.3	13.9	17.2	9.0	7.5	9.1
1100 °C	100% CO	30	115	42	73	36	26	46.5
	CO/CO ₂ =1	20	36	25	38	23	15	27.0
	CO/N ₂ =1	27	70	33	45	23.2	19	30.5

Table 1: The effect of impurity oxides on the initial rate of zinc oxides at 900 °C, 1000 °C and 1100 °C respectively.

The average pore sizes at or near the reaction interface (e.g., diameter and spacing of the tunnels) observed in these SEM microstructures are found to be dependent upon the partial pressure of reducing gas, reaction temperature, and type of impurity oxide additions. For example, the average pore size measured at or near the reaction interface by SEM increased with dissolved impurity oxides in solid solutions in this order: MgO, Al₂O₃, SiO₂, MnO and CaO (i.e. pore size ranges from 0.1 μm to 2 μm). The more porous structure formed with MnO and CaO additions also coincide with observations of higher reduction rate relative to pure ZnO reduction.

No significant differences in product morphologies are observed in all the reduced ZnO solid solution samples studied at all reduction temperatures and reducing gas mixtures employed. The tunnels or fibrous-like elongated pores extend right up to the reaction interface and are roughly perpendicular but oriented to the advancing reaction interface.

From microstructure evidence and kinetic data, the author [5] has shown that the contribution of pore diffusion resistance is more significant with finer pore size when compared with coarser pore structure. For example, for the reduction of ZnO containing 3 wt% dissolved FeO in pure CO, the ratio of the effective diffusivities at reduction temperature of 900 °C and 1000 °C, $D_e(900^\circ\text{C})/D_e(1000^\circ\text{C})$, was estimated to be 0.249, substantiating the view that the resistance to pore diffusion of reducing gas becomes more significant with finer pore structure. All ZnO solid solutions studied showed finer pore sizes close to the reaction interface but the average pore sizes increase towards the external sample surface. The presence of coarser intergranular pores generated along the grain boundaries in addition to the finer pore structure formed within the grains were observed with dissolved CaO, MnO and SiO₂ in ZnO solid solution; the presence of grain boundary reductions further increased the reduction rate due to shortening of diffusion distances (i.e., more porous pore structure) compared with other dissolved impurity oxides (Al₂O₃, FeO, and MgO). These results are consistent with the higher rate of reduction of ZnO containing dissolved CaO, MnO and SiO₂ (in this order) when compared with other dissolved impurity oxides (Table 1).

The overall external dimensions of the reduced pellets with dissolved impurity oxides of Al₂O₃, FeO, MgO, MnO, CaO and SiO₂ in zinc oxide solid solution were found not to change significantly as reduction proceeds. Each sample followed a well-defined shrinking-core pattern upon reduction reaction, with the formation of fibrous-typed porous product layer as the reaction interface advances into the dense bulk oxide.

Discussion

During reduction with CO reducing gas, ZnO solid solutions decomposed into Zn (g) and CO₂ to the bulk gas phase and the dissolved impurity oxide (Al₂O₃, MgO, CaO, MnO, FeO, Fe and SiO₂) partitioning to the impurity oxide phase forming the longitudinal pore walls of the reaction product morphology. That is, the reduction of ZnO solid solutions lead to the formation of elongated pore tunnels at the reaction interface. The impurity oxide/metal precipitates were rejected at the reaction interface during reduction. The precipitates grow out from the reaction interfacial surface in the form of plate-like needles without spreading laterally across the ZnO surface as the reaction interface advances into the bulk oxide sample. The thickness layer of the reaction product morphology increases with the progress of reduction; and consequently the resistance to diffusion of reducing gas across the pore structure increases, which therefore decrease the rate of reduction.

Analysis of Rate Data

An assessment of whether chemical kinetics, pore diffusion and external mass transfer resistance constitute the rate controlling step for ZnO solid solutions was possible by examining and plotting the rate data in the form of (Szekely *et al.* [6]):

$$At = 1 - (1-X)^{1/3} + \sigma_s^2 \left\{ 1 + 2(1-X) - 3(1-X)^{2/3} \right\}$$

where, X = overall fractional conversion of solid reactant, and

$$\sigma_s^2 = \frac{k}{2D_e} \left(\frac{V}{A} \right)$$

$$A = \frac{k}{p_s} \left(\frac{A}{3V} \right) (C_{\text{CO}, b} - C_{\text{CO}, s})$$

which takes into account of the gas diffusion of reducing gas through the reaction product layer and chemical reaction on the reaction interface. For the gas flows employed in the experimental condition studied, the reaction resistance due to external mass transfer is negligibly small; the gas composition near the surface of the particle attains a value close to that of the bulk gas phase. For example, the calculated mass transfer rate was found to be $2.43 \times 10^{-4} \text{ mol cm}^{-2} \text{ s}^{-1}$ for reduction reaction with pure CO ($P_{\text{CO}}^e = 0.6829 \text{ atm}$) at 1000 °C [5]. The measured reduction rates of 1 wt% of CaO and MnO in ZnO solid solutions were $8.680 \times 10^{-6} \text{ mol cm}^{-2} \text{ s}^{-1}$ and $5.144 \times 10^{-6} \text{ mol cm}^{-2} \text{ s}^{-1}$ respectively [5]. Hence, the external mass transfer rates are much larger than the chemical reaction rates in the temperature range studied.

Therefore, the experimental results are analyzed by plotting $1-(1-X)^{1/3} + \sigma_s^2 [1 + 2(1-X) - 3(1-X)^{2/3}]$ against time (this is referred to as the mixed control plot). The effective diffusion coefficient of gas through the reaction product

layer, D_e , and the specific rate constant of interfacial chemical reaction, k , are calculated to estimate the value of σ_s^2 (Lee & Hayes [3]). In the case where σ_s^2 cannot be computed from D_e and k (i.e. where the reaction product morphology formed is not well defined to calculate the pore diffusion coefficient, D_p , and the fractional porosity, ϵ), then the solution is by substituting experimental values of t for two values of X in a narrow range and solving for σ_s^2 ; the average values of σ_s^2 can then be calculated by a computer program from experimental data for the entire reduction process.

Typical examples of mixed control plots for reduction experiments of 1 wt% of MnO, FeO, CaO, SiO₂, Al₂O₃ and MgO are shown in Figure 4.

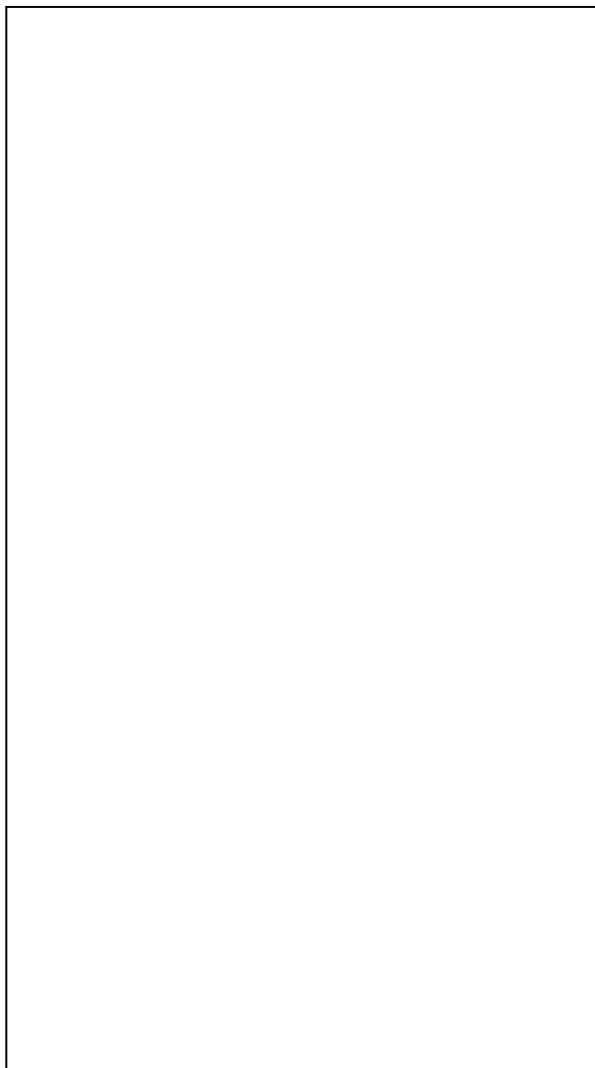


Figure 4. Typical examples of mixed control function, $F(x)$, against time plot for the reduction of ZnO solid solutions. [$F(x) = 1 - (1-X)^{1/3} + (\sigma_s)^2 \{1 + 2(1-X) - 3(1-X)^{2/3}\}$]. (a) 1wt% MnO, 1273K; (b) 1 wt% FeO, 1173K – 1373K; (c) 1wt% CaO, SiO₂, Al₂O₃, MgO at 1273K.

The results clearly indicated the linear relationships for the reduction reactions for all reduction temperatures and reducing gas mixtures studied. The transition from chemical reaction control to pore diffusion control as the reduction progresses is dependent on reduction temperature, gas composition, type of impurity addition and degree of reduction. In all cases, when the porous product layer acquires sufficient thickness, pore diffusion of reducing gas through the reaction product layer ultimately becomes the main rate-controlling process, i.e. $X > 0.48$. The relative contribution of chemical reaction during the initial stages of reduction is at its maximum and decreases gradually as the thickness of the reaction product layer grows. That is, CO must now diffuse through a progressively increasing thickness of porous product layer to react with a progressively receding non-porous unreacted core of ZnO solid solution.

Table 2 shows some calculated experimental values of k , σ_s^2 , and \dot{A} for the reduction of pure ZnO, and ZnO containing 1 wt% of CaO, MnO and FeO at selected reducing gas mixtures and at 1000 °C. In this study, the calculated values of σ_s^2 in all experimental conditions studied were found to lie in the range from 0.1 to 10. These results indicate, according to criteria for σ_s^2 developed by Sohn and Wadsworth [7] that the reduction process is influenced by chemical reaction and pore diffusion of reducing gas through the reaction product layer.

The values of the calculated chemical reaction rates of all the dissolved impurities in ZnO solid solutions studied were also found to be approximately equal to the measured initial linear reduction rates, thus substantiating the argument of chemical reaction controlled during the initial stage of reduction reaction; the contribution of pore diffusional effects is considered small for all practical purposes when $X < 0.3$. The average pore sizes generated during reduction reaction determines the transition from one limiting rate controlling processes to another and this is dependent upon the type of impurity additions, partial pressure of reducing gas, and reduction temperature. From the above analysis, it can be concluded that the overall resistance to the reduction process of ZnO containing 1wt% of Al₂O₃, FeO, MgO, CaO, MnO and SiO₂ treated with CO/CO₂ and CO/N₂ gas mixtures at reduction temperature ranges from 900 °C to 1100 °C is controlled jointly by chemical reaction and pore diffusion of the reducing gas through the reaction product layer. For the most part, the reduction process is dominated by the pore diffusion. In the initial stage ($X < 0.3$), the resistance offered by the chemical reaction is significant.

		Pure ZnO	1 wt% CaO	1 wt% MnO	1 wt% FeO
100% CO	$k \text{ cms}^{-1}$	0.330	7.208	1.847	0.595
	σ_s^2	0.267	0.480	0.544	1.167
	$\dot{A} \text{ s}^{-1}$	-	6.668×10^{-3}	1.709×10^{-3}	5.505×10^{-4}
CO/N ₂ = 1	$k \text{ cms}^{-1}$	0.366	1.787	0.483	0.137
	σ_s^2	0.331	0.396	0.387	0.638
	$\dot{A} \text{ s}^{-1}$	-	3.473×10^{-3}	9.390×10^{-4}	2.667×10^{-4}
CO/CO ₂ = 1	$k \text{ cms}^{-1}$	0.370	1.607	0.400	0.132
	σ_s^2	0.378	1.717	0.490	0.621
	$\dot{A} \text{ s}^{-1}$	-	2.873×10^{-3}	7.143×10^{-4}	2.367×10^{-4}

Table 2: Selected values of k , σ_s^2 and \dot{A} obtained from the reduction of zinc oxide solid solutions at 1000°C.

Mechanism of Microstructure Formation For ZnO Solid Solution

The gaseous reduction of ZnO solid solutions, (Zn,M)O, involve the removal of zinc and oxygen atom by chemical reaction with the reducing gas and the simultaneous precipitation of M-metal or M-oxide at the reaction interface. The notation M represents either one of these ions homogeneously incorporated into the ZnO lattice structure; Fe²⁺, Mg²⁺, Ca²⁺, Mn²⁺, Si⁴⁺ and Al³⁺ ion. The changes within the system during reduction reaction includes:

1. An increase in the impurity level or M ion concentration with the eventual supersaturation of the oxide; and
2. The nucleation and growth of more stable product phase.

[Zn] and [O] removal from the oxide surface by chemical reaction with the reducing gas increases the local M ion concentration at the reaction interface; this increase in M ion concentration sets up a concentration gradient for the diffusion of M ions into the bulk solid. The change in surface composition with the progress of reduction is primarily dependent upon the relative rates of chemical reaction and M ion mass transport sub-processes. Nucleation of the more stable product phase occurs when the oxide surface becomes supersaturated with M ions. The number and distribution of these nuclei depends on the oxide surface; edges of low energy faceted planes, instabilities, lattice defects and surface irregularities are examples of high energy sites that greatly favored the formation of nuclei (Christian [8], Bogdandy & Engell [9]).

The most striking feature for the reduction of (Zn,M)O is the formation of reduction tunnel structure extending from the reaction interface to the reaction product surface observed under all experimental conditions studied. This type of

morphology (Figure 3) which is drawn schematically in Figure 5, shows (Zn,M)O decompose with the M-metal or M-oxide partitioning to form the pore walls and, zinc and oxygen to the bulk gas phase. In all cases of the SEM micrograph observed, the oxide at the pore tip is directly exposed to the reaction gas and surrounded by M-metal or M-oxide scale, and hence the actual reaction interfaces encountered for the reduction of ZnO solid solution core basically the same and therefore can be discussed concurrently with a single reaction model. The pores allowed the reducing gas to diffuse to the advancing reaction interface for chemical reaction. However, for the reaction to proceed, short-range solid state diffusion of M cations (J_M) at or near the reaction interface to the points of the growing nuclei from the points where zinc and oxygen removal occurs is necessary.

The mechanism of attachment of M atoms to the growing nucleus can occur in a number of ways. By depositing and sintering trace amount of CaO particles ($\geq 1 \mu\text{m}$) into the dense, unreduced (Zn,Si)O solid solution external sample surface (e.g. 30 min. at 1200 °C in 50% N₂-50% O₂), and then subsequently reducing the sample for 1 min with 10% CO-90%N₂ gas mixtures, the author [5] has shown that the CaO particles continued to remain on top of the growing filament of SiO₂ precipitates as the reaction interface advances into the unreduced bulk oxide. The M atoms are therefore attached directly from the bulk of the ZnO solid solution to the base of the growing nucleus at the M-oxide/(Zn,M)O or Fe/(Zn,Fe)O interface; the stable nucleus will increase in height as the reaction interface advances into the bulk oxide. Additionally, if the rate of atom attachment at the perimeter of the nucleus from the oxide surface is greater than the rate of advance of the gas/oxide interface (i.e., rate of pore growth), then the nuclei will eventually spread across the surface; however, this type of

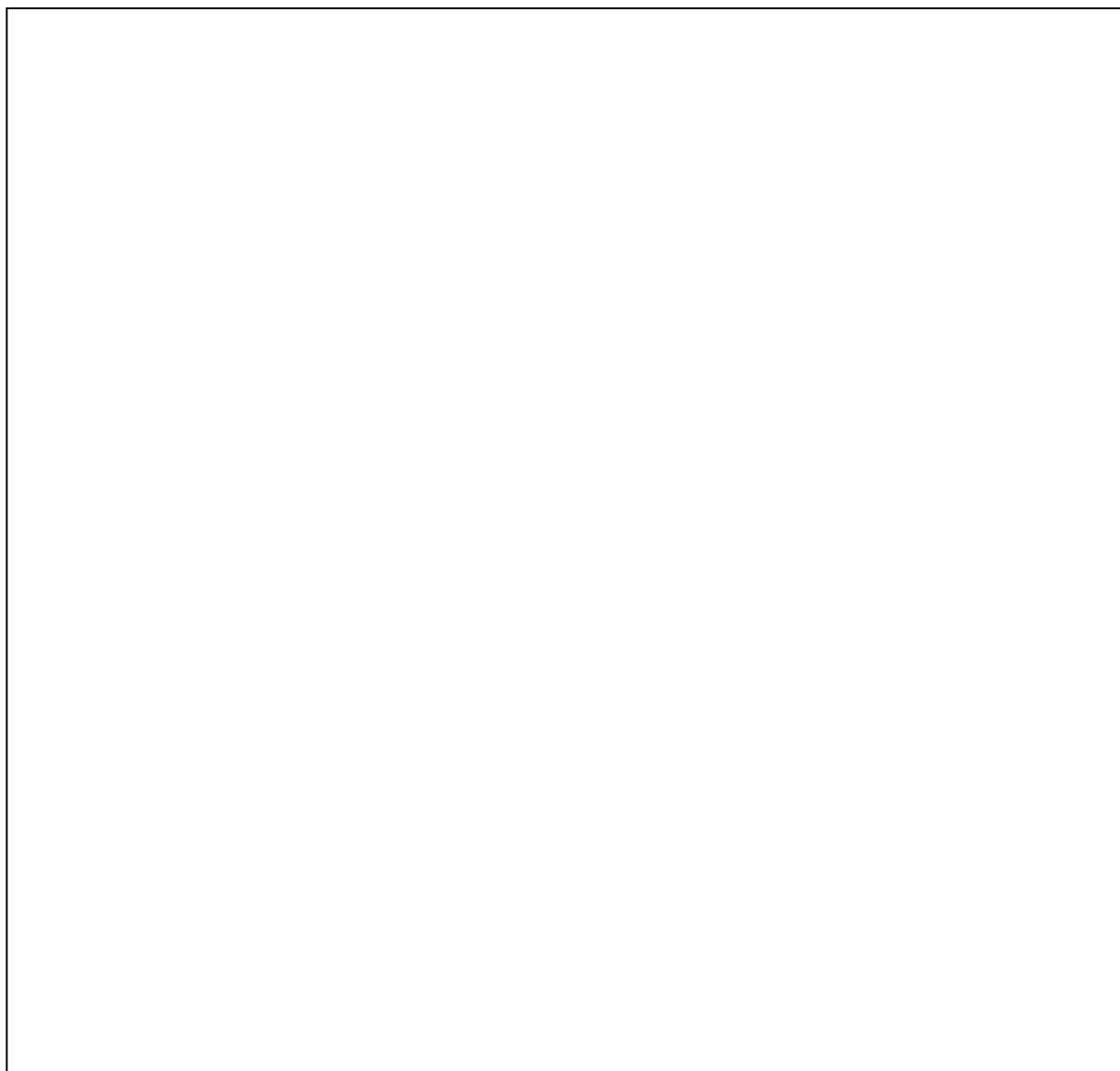


Figure 5. Schematic diagram showing the various stages of nucleation and growth of impurity oxides during reduction of ZnO solid solutions. [M] = Fe²⁺, Mg²⁺, Ca²⁺, Mn²⁺, Si⁴⁺, or Al³⁺ ion.

reaction mechanism was not observed microscopically at all reduction conditions and for all the dissolved impurities studied.

The M ions can diffuse rapidly within the network of the ZnO lattice structure; the diffusivity of M cations in ZnO depends on the ionic charge and ionic radius (Hauffe and Vierk [10]) and this also influences the rate of reduction of ZnO. Figure 5 illustrates the various stages involved in the formation of pore tunnel structure during the reduction of (Zn,M)O solid solutions based on observed microstructural evidence. The initial stage of decomposition prior to [M] nucleation during reduction reaction at gas/solid interface is shown in Figures 5(a-c); the symbol [M] represents a metal ion that is homogeneously distributed in solid solution. The lines on the figures indicate equal level of M ion concentration in the solid structure. The removal of oxygen and zinc atoms from the (Zn,M)O surface increases the local M ion

concentration at this interface.

The resulting chemical potential gradient created in the solid structure leads to M ions diffusion into the bulk solid, however the actual increase in surface concentration and M ions distribution are dependent upon the relative rates of the various chemical reaction and mass transport sub-processes; the maximum gradient for which is normal to the M ion concentration profile. The net M ion flux is normal to the original surface during planar decomposition (Figure 5(a)). However, the formation of surface perturbation (Figure 5(b)) resulted from the removal of [Zn] and [O] atoms in the concave interface, and lateral rejection of M ions in directions parallel to the original interface. As the reduction progresses, the increase in M ion concentration in the oxide ahead of the perturbation is lower than the adjacent planar surface. Thus the surface composition at the pore tip is furthest removed from equilibrium with the gas, and hence

the chemical reaction is fastest at this point than on a planar surface. The difference in decomposition rates continues as the oxide is reduced and results in the surface becoming unstable and forming pores into the bulk solid (Fig. 5(c)). The formation of instabilities is favored by the presence of structural defects, such as grain boundaries or dislocation, since these represent preferential profiles due to their effect upon the local ionic mobilities.

The depth of the perturbation is determined by the relative rates of chemical reactions, pore diffusion of reducing gas, surface diffusion and bulk mass transfer of M ions. Larger differences between the surface and bulk compositions (especially during the early stage of reduction reaction) will result in high rates of instability formation and hence greater depth of perturbation or curvature below the outer surface.

As reduction proceeds, the composition of (Zn,M)O in contact with the reducing gas becomes richer in M ions until eventually supersaturation is reached with the oxide surface in a metastable condition. That is, the activity of M ion is highest at the oxide surface and increases with the progress of reduction, eventually exceeding that of M metal or M-oxide (unity) and creating a supersaturated and unstable region below the surface. When the surface activity of M ions reaches a critical value, which is high enough locally for nucleation, the oxide decomposes to form a more stable nucleus (e.g. precipitates of Fe, FeO, Al₂O₃, SiO₂, MgO, MnO, CaO) and (Zn,M)O of a lower M ion concentration. The activity of M-metal or M-oxide in the nucleus is unity and M ion can diffuse back, from the supersaturated (Zn,M)O solid solution towards the nucleus, thus causing it to grow (Fig. 5(d)). The zinc and oxygen removal by the reducing gas continues during this process.

Following the nucleation of M-metal or M-oxide, the excess M ions in the supersaturated (Zn,M)O solid solution in the proximity of the nucleus will result in a large flux of M ions to the nucleus via surface and bulk diffusion. Precipitation of these M ions in the existing nucleus as reaction interface advances into the bulk oxide results in a relative increase in the height of the nucleus and a decrease in the local M ion concentration of the oxide; however, zinc and oxygen removal from the system by chemical reaction with the reducing gas continues this process (Fig. 5(e)). Following growth of reaction product layer, the relative rate of M atom attachment to the base of the pore wall and the rate of growth of perturbation determines the degree of curvature and growth behavior of the precipitated oxide filaments; this is dependent upon the chemical reaction rate at the reaction interface and hence the pore diffusion rate of reducing gas through the porous layer.

The interface reaction model proposed in Figure 5(e) involves the net removal of zinc and oxygen from the pore and the incorporation of the excess M ions generated into the precipitated (oxide or metallic) phase. Examining Figure 5(e), the extraction of zinc and oxygen atoms from the (Zn,M)O lattice by CO reducing gas generates an excess of M ions in the surface and leads to M ion diffusion. The excess M cation generated on the pore tip will have to diffuse to the metal or metal oxide sink under the local concentration gradient created. Simultaneously, in order for the reaction interface to advance into the bulk oxide, both oxygen and zinc must be removed from the [MO]/(Zn,M)O interface and pore interface (i.e. gas/(Zn,M)O interface) while the M cation produced there are deposited on the precipitated [MO] product phase, where [MO] represents the following metallic or oxide phase: i.e., Fe, FeO, Al₂O₃, MnO, CaO, SiO₂, MgO). If the product layer [MO] is to grow and have a continuous longitudinal pore tunnel arrangements, then the [MO]/(Zn,M)O and gas/(Zn,M)O interfaces must both move to the bulk oxide at equal rates as reduction reaction proceed. Oxygen and zinc ions at the [MO]/(Zn,M)O interface has to diffuse to the pore surface for this reduction reaction to proceed.

Conclusions

The reduction of dense ZnO solid solutions in CO/CO₂ and CO/N₂ gas mixtures has been investigated at temperatures between 900 and 1100 °C. The rate measurements obtained in these studies were complemented with the microstructural characterization of the reacted and partially reduced samples.

The experiments have demonstrated that the kinetics of reduction of zinc oxides were directly dependent upon the CO partial pressure, temperature, degree of reduction, and the type of impurity oxides added (i.e. FeO, MgO, CaO, SiO₂, MnO, and Al₂O₃) into the samples. The results of the percentage reduction against time plots showed an initial linear reduction rate followed by a decrease in rates as reduction proceeds. The reduction rates were also found to increase with increasing temperature and CO partial pressure. Generally, greater reaction rates were observed for samples reduced in CO/N₂ gas mixtures than with CO/CO₂ gas mixtures for comparable CO partial pressure.

The reduction rate of ZnO in CO/CO₂ and CO/N₂ gas mixtures was found to increase by the addition of CaO and MnO in solid solution whereas the incorporation of MgO and FeO generally decreases the rates significantly. Other impurity oxide additions showed intermediate values and/or similar relative reduction rates to pure ZnO reduction.

A simplified interface reaction model has been proposed for the observed reaction kinetics and product microstructures formed for the reduction of ZnO solid solutions. From the analysis of the relative rates of the various chemical reactions and transport processes, it can be concluded that the rate of reduction of zinc oxide was controlled jointly by chemical reaction at the ZnO surface and pore diffusion of reducing gas through the porous ZnO/product layer. The relative contributions from chemical reaction and pore diffusion rates were found to be related to the average pore sizes and reaction time.

Acknowledgement

The author would like to thank the University of Queensland and Pasminco Limited, Boolaroo, NSW 2248, Australia for providing the financial support that enabled completion of this research work. The author would also like to thank Assoc. Prof. Peter Hayes for his advice and valuable comments.

References

1. Jones, T.S., and Davis, H.M. (1967) "Reduction of ZnO by CO in the Presence of Strontium Oxide", *Trans. AIME*, **239**, 244-248.
2. Guger, C.E., and Manning, F.S. (1971) "Kinetics of ZnO Oxide Reduction with Carbon Monoxide", *Metall. Trans.*, **2**, 3083-3090.
3. Lee, F.T., and Hayes, P.C. (1991) "The Reduction of Zinc Oxide", *5th Aus. IMM*

Conference on Extractive Metallurgy, Murdoch University, Perth, 263-268.

4. Matthew, S.P., St. John, D.H., Hardy, J.V., and Hayes, P.C. (1986) "Techniques for the Preparation and Examination of Partially Reduced Oxides", *Metallography*, **18**, 367-379.
5. Lee, F.T. (1990) "The Reduction of ISF Sinters", Ph.D. Thesis, The University of Queensland, Brisbane, Australia.
6. Szekely, J., Evans, J.W., and Sohn, H.Y. (1976) "Gas-Solid Reactions", Academic Press, New York.
7. Sohn, H.Y., and Wadsworth, M.E. (1979) "Rate Processes of Extractive Metallurgy", Plenum Press, New York, 313.
8. Christian, J.W. (1975) "The Theory of Transformation in Metals and Alloys": Part 1, 2nd ed., Pergamon Press, Oxford.
9. Von Bogdandy L., and Engell, H. J. (1971) "The Reduction of Iron Ores", Springer-Verlag: Berlin and New York.
10. Hauffe, K., and Vierk, A.L. (1950) "Electrical Conductivity of ZnO doped with Foreign Oxides", *Z. Phys. Chem.*, (Wiesbaden), **196**, 160-180.
11. Lee, F.T. (2000) "Phase Equilibrium Studies for the ZnO-Fe₂O₃-CaO-SiO₂ Quaternary System of Zinc Blast Furnace Sinters", *Journal Institution of Engineers, Malaysia*, **61 (3)**, 29-